Heliyon 8 (2022) e10345

Contents lists available at ScienceDirect

Heliyon

journal homepage: www.cell.com/heliyon

Research article

Smart apparel using nano graphitic carbon nitride/PVA in a cotton cloth for military application

Srimathi Krishnaswamy [a,*], Puspamitra Panigrahi [a], Praseetha Prabhakaran Kala [b], Sharon Sofini [b], Ganapathi Subramanian Nagarajan [c,**]

[a] Centre for Clean Energy and Nano Convergence (CENCON), Hindustan Institute of Technology and Science (HITS), Padur, Kelambakkam, Chennai 603103, India
[b] Noorul Islam College of Engineering, Noorul Islam Centre for Higher Education, Kumaracoil, Kalkulam, Thucklay, Tamil Nadu 629180, India
[c] Quantum Functional Semiconductor Research Centre (QSRC), Nano Information Technology Academy(NITAs), Dongguk University, 30 Pildong-ro 1-gil, Jung-gu, Seoul 04620, South Korea

ARTICLE INFO

Keywords:
GCN
PVA thin Film
Nanocomposite
Smart apparel
Bandgap
Flexible electronics

ABSTRACT

An eco-friendly, low-cost smart attire was made of metal-free graphitic carbon nitride (GCN) as a semiconductor material in a biodegradable synthetic polymer (polyvinyl alcohol) and cotton material. Various concentrations such as 0.04, 0.08, 0.12, 0.16, and 0.2 weight percentage of GCN is entrenched in PVA. UV absorption spectra displayed two peaks, one matching PVA (317 nm) and the other excitonic peak of GCN (390 nm).0.2% GCN in PVA showed a low bandgap (2.84 eV) harnessing maximum solar light. Due to the charge transfer mechanism, enhanced blue emission at 450 nm was observed for the higher concentration of graphitic carbon nitride. Due to more defect centers of higher weight percentage of GCN, higher electrical conductivity (7.6462×10^{-3} S/cm) and optical conductivity (0.113 S) were noticed. Due to the higher conductivity of 5GCN, it was embedded with cotton fabric. The fabricated smart apparel can be used to manufacture flexible, lightweight, eco-friendly optoelectronic devices. Further, according to literature, GCN possesses high antibacterial activity, hence it can serve as clothing for the military and medical community.

1. Introduction

In the recent decade, wearable electronics have attracted significant interest in scientific society owing to their intrinsic properties [1]. Fiber-based clothing system has been used by humans for a long ago due to their durable, breathable, and washable nature and it is an ideal material for wearable electronics. On the other hand, nanotechnology has gained widespread application in electronic devices. Nowadays, it is possible to construct electronic devices on the surface of cloth. Owing to the structure of fiber assemblies, fiber electronics possess excellent fatigue resistance which makes an excellent area of research for wearable electronics and found promising applications such as flexible circuits, skin-like pressure sensors, radiofrequency identification tags, personal electronics, biomedical and antimicrobial textiles, and military garment devices [2, 3, 4, 5, 6]. In wearable electronics, materials such as metal oxide particles, conductive polymers, and carbon nanotubes are used as fabricated electronics devices and sensors [7].

In transient electronics, natural wax, silk, polycaprolactone, polylactic acid, cellulose derivative, and polyvinyl alcohol (PVA) are used [8, 9]. Among these materials, PVA is a water-soluble, economical, and biocompatible polymer [10, 11]. The optical, electrical, and mechanical properties of the PVA can be tailored by adding dopants (organic/inorganic) to the polymer matrix. This composite has found various applications such as 3D printing, coatings, and optoelectronic devices [12, 13]. On the other hand, metal conductors (e.g Fe, W, Mo, Zn, and Mg) [14] and semiconductors such as ZnO, Si, and Ge [15] are incorporated in PVA and used in transient electronics. As PVA contains –OH groups which can interact with other molecules (inorganic and organic materials) to form a PVA composite [16]. Alkali-halide salt was incorporated in PVA thin film by Suchkova et al [17] and investigated the luminescence properties. An enhanced luminescence was observed due to the interaction of vacancy defects on alkali halide salt microcrystals. On the other hand, Graphene was added to PVA by an electrospinning process [18]. The nanocomposite thin film exhibited higher conductivity when compared to pure PVA. This material can find applications as

* Corresponding author.
** Corresponding author.
E-mail addresses: ksrimathi@hindustanuniv.ac.in (S. Krishnaswamy), ganapathi@dongguk.edu (G.S. Nagarajan).

https://doi.org/10.1016/j.heliyon.2022.e10345
Received 14 November 2021; Received in revised form 2 February 2022; Accepted 12 August 2022

transparent electrode material for optoelectronic devices and supercapacitors [19]. Despite these astonishing advances in flexible electronics still, the choice of material is limited due to its cost and fabrication techniques. Hence a low-cost material is needed for electronics.

The metal-free earth-abundant graphitic carbon nitride (GCN) has the properties of graphene and it is a cost-effective material that has great interest to researchers all over the globe [20]. This material acts as a photocatalyst due to its high thermal and chemical stability [21]. GCN has tri-s-triazine ring structure with a high degree of polymerization. It possesses a suitable bandgap (2.6 eV) with a conduction band position at 1.07 eV. GCN has sufficient –NH functional groups which act as active sites for robust interface bonding with polymer matrix [22]. Due to these amazing properties, GCN-based nanocomposites have been used in the field of photocatalysis, energy storage, bioimaging, and energy storage applications [23, 24, 25, 26, 27].

Interestingly, Fan et al [28] embedded GCN nanosheets onto cotton fabric using the electrostatic interaction method and evaluated the photocatalytic degradation of rhodamine B dye under simulated sunlight irradiation. The modified apparel exhibited great durability and was reused for further catalytic performance. Nemati et al [29] fabricated PVA-based nanofiber with GCN/cellulose/nettle and trachyspernum by electrospinning method and found application in wound healing. After 14 days, the nanofiber exhibited of higher wound healing percentage of 95%. He et al [30] synthesized GCN/PVA nanocomposite thin film through the casting method and studied the mechanical properties [Table 1].

Inspired by this strategy, a facile method has been developed to fabricate optically transparent PVA/GCN film in the present study. So far in the literature, the optical properties of PVA/GCN were not discussed. Therefore, we fabricated PVA/GCN nanocomposite thin film and studied all its properties. Further, the optimized PVA/GCN composition was cast on cotton and studied the optical properties.

2. Experimental

2.1. Synthesis of GCN particles

The alumina crucible with lid is washed with ethanol and dried and added urea (10 g) to it and kept crucible in a muffle furnace [21]. The furnace is heated at a rate of 5 °C/min to attain 500 °C and it is maintained for 2 h and cooled to room temperature. The material was ground in mortar and pestle and collected in a sample vial. The obtained material was in light yellow color and labelled as GCN.

2.2. Fabrication of nanocomposite thin film

10 g of PVA is dissolved in 100 ml of distilled water in a 250 ml beaker and heated at 70 °C for 2 h with stirring using a magnetic stirrer. After cooling to room temperature, the PVA solution is cast on the cleaned glass substrate and cooled for 2 days at room temperature. Prior to coating, the glass plate was cleaned with soap solution, distilled water, and methanol and dried the glass plate in the oven at a temperature of 70 °C. Different concentrations of GCN (0.04, 0.08, 0.12, 0.16, and 0.2 weight percentage) were added to 5 g of PVA solution and mixed thoroughly. Further, the solution was cast on a glass substrate and left to air-drying for 3 days. The prepared nanocomposite thin film from 0.04, 0.08, 0.12, 0.16, and 0.2 weight percentage of GCN in PVA was designated as 1GCN, 2GCN, 3GCN, 4GCN, and 5GCN respectively. GCN is infused by the dispersion process in the PVA polymer matrix such that GCN particles are completely captured by the polymer. Functional groups such as $–NH_2$ and –NH are present in the terminal position of GCN. The –OH group in Polyvinyl alcohol reacts with these functional groups ($–NH_2$ and –NH) of GCN through Van der Waals force and hydrogen bonding to form a strong bond (Red bond-Figure 1). By the gravimetric method, the thickness of the thin film was measured by using Eq. (1) [31].

$$T = m/\rho \times A \quad (1)$$

m – The mass of the deposited thin film
A – area of the deposited thin film
ρ – density of the deposited material

2.3. Fabrication of GCN/PVA on cotton fabric

By casting technique, 5GCN solution was applied on cotton cloth using a glass rod. The nanocomposite material was applied to the cotton cloth uniformly and left at room temperature for 48 h s for drying. The prepared cotton fabric was taken for analysis.

2.4. Characterization

The structural analysis was performed using X-ray diffraction (XRD) (SEIFERT-2002 model, DYEFLAX, Germany) with Cukα radiation (λ = 1.5412 Å). The morphology of the GCN powder was investigated using a scanning electron microscope (SEM, COXEM, CX 200TA Model) was employed. UV visible spectrophotometer (Shimadzu double beam monochromator spectrophotometer UV-2450). JASCO 8660 is used for optical studies. spectrofluorometer was used to study photoluminescence (PL) studies. Perkin Elmer model TGA 7 was used to study the thermal properties. The heating range is in the range of 20 °C to 800 °C at 2 °C/min in the nitrogen atmosphere. Hall effect measurement (Ecopia HMS 3000) system is used to study the electrical conductivity of the thin film. The sample size for the hall effect is 1 cm × 1 cm (glass plate). For the validation of the result, the electrical conductivity of the GaN thin film (supplied by the Ecopia) was tested each time. Microtrac MRB analyzer to investigate the particle size.

3. Result and discussion

3.1. Analysis of GCN particles

The structural properties of GCN were investigated by XRD. Two peaks were noticed for the GCN particles (Figure 2a). The peak at 12.99° is attributed to the 110 peak which is due to the tris-s-triazine of the in-plane structure and further, the repeated unit has d spacings of 0.712 nm [32]. The second peak at 27.89° is the 002 peak which is accredited to the aromatic system stacking plane. The conjugated system exhibited a d spacing of 0.323 nm [32]. The formation of graphitic-like structures was confirmed in XRD analysis. Figure 2b depicts the thermal studies of GCN particles. The GCN particle starts decomposing above 500 °C and complete degradation happens at 600 °C [33]. As GCN is stable up to 500 °C it can be fused with PVA polymer [32]. Hence, the synthesized sample was taken further to make thin-film composites. Figure 2c depicts the absorbance of the GCN sample. A broad peak at 424 nm was observed in the visible region of the solar spectrum. The absorbance is due to the transfer of an electron from the highest occupied molecular orbital (HOMO) to the lowest unoccupied molecular orbital (LOMO) of the π-π* in the GCN molecule. Further, the room temperature photoluminescence of the GCN particle is investigated in detail. Figure 2d depicts the PL emission of GCN which on excitation at 325 nm emits radiation at 444

Table 1. Literature survey of GCN composite.

Material	Method of synthesis	Application	Reference
GCN/cotton cloth	electrostatic interaction method	Dye degradation	28
GCN/cellulose/nettle and trachyspernum in PVA	electrospinning method	Wound healing	29
GCN/PVA	casting method	Mechanical property	30

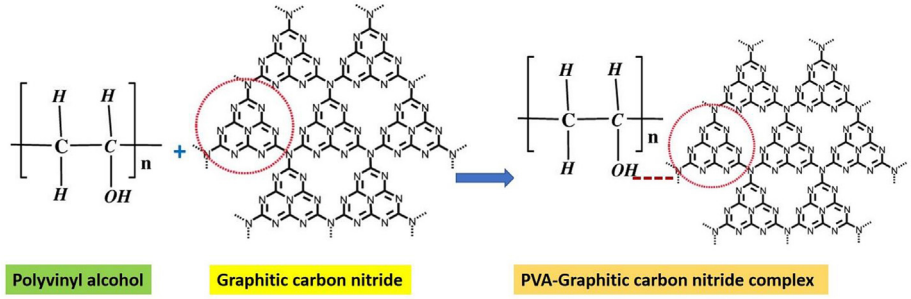

Figure 1. Schematic representation of the formation of PVA-GCN complex.

nm. The PL emission of GCN is due to the π-π* electronic transitions [33] and nitrogen incorporation in the polymeric units.

3.1.1. Morphology and particle size

The morphology of GCN particles was studied by SEM analysis. Figure 3a depicts the SEM of pure GCN particles. A layered structure is noticed for GCN particles which are comparable to graphene structure. MRB analyzer is used to determine the particle size. Figure 3b depicts the statistics graph of particle size distribution which depicts the particle size as 10.3 nm. The particle analyzer depicts the nanostructure formation of GCN.

3.2. Nanocomposite

3.2.1. Structural analysis

The XRD of PVA/GCN is depicted in Figure 4a. All the thin films show a broad diffraction peak at 19.5° which is due to the semi-crystalline nature of PVA [30]. The characteristic peaks of GCN are not observed due to the low content of GCN in the polymer matrix. Further, the crystal structure of PVA has not changed due to the presence of GCN in the nanocomposite thin film.

3.2.2. FTIR studies

The interaction between GCN and polymer was studied in detail by using FTIR transmission spectra [Figure 4b]. For pure GCN, the peak at 860 cm^{-1} corresponds to the breathing vibration of triazine units [34]. The peaks from 1200 to 1640 cm^{-1} indicate the stretching vibration of GCN heterocycles [35]. The weak peak at 2300 cm^{-1}may be due to the absorption of CO_2 molecules on the surface [35]. The peak above 3000 cm^{-1} corresponds to the N–H stretching vibrations of primary and secondary amines [35, 36, 37]. As per the literature, the peaks 700–1500 cm^{-1} corresponds to pure PVA thin film [38]. The peaks at 1076 cm^{-1}, 1405 cm^{-1} and 840 cm^{-1} of nanocomposite thin film correspond to C–C, CH_2 and C–O stretching of PVA [38]. The peaks at 3529 and 1660 cm^{-1} correspond to stretching and bending vibrations of O–H bond in PVA [38]. By comparing the bare GCN and GCN/PVA composite the broad peak at 3739 cm^{-1} is shifted to the lower wavelength of 3663 cm^{-1} indicating the interaction of PVA and GCN. The surface passivation of PVA through GCN was affirmed by the intermolecular hydrogen bonds between –N–H of GCN and –O–H of the PVA matrix.

3.2.3. Optical studies

Figure 5a exhibits the absorbance spectra of the nanocomposite thin films. Two absorbance peaks were noticed for all samples. The first peak at 317 nm corresponds to the n-π* and π-π* of the PVA matrix [39] and another peak at 390 nm corresponds to the π-π* of the GCN particle [38]. In Figure 5a, the broad peak is due to the synergistic effect of π-π* transitions in PVA and GCN. The thin-film optical properties are mainly dependent on the dopant percentage and size of the nanoparticle embedded. Therefore in the current study, with an increase in the

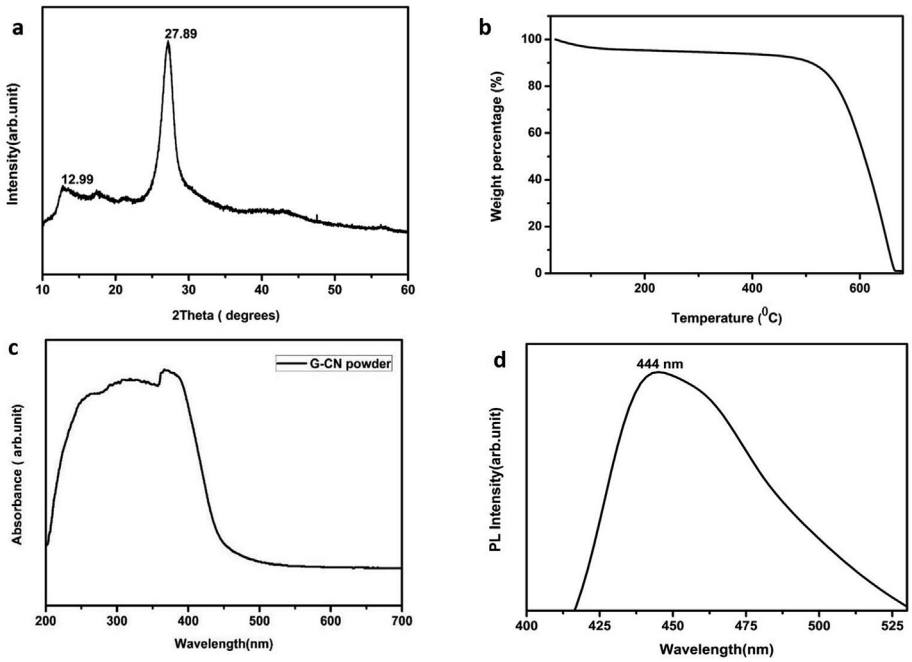

Figure 2. (a) XRD of GCN sample, (b) TGA of GCN sample (c) UV absorbance of GCN sample, (d) Room temperature of GCN sample.

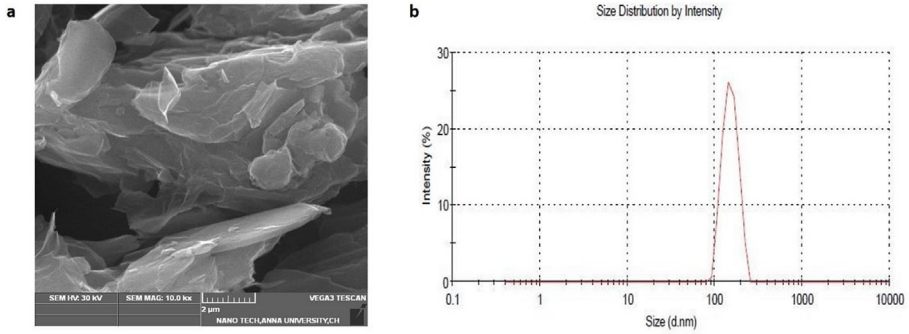

Figure 3. (a) SEM of GCN particle, (b) Particle size distribution of GCN particle.

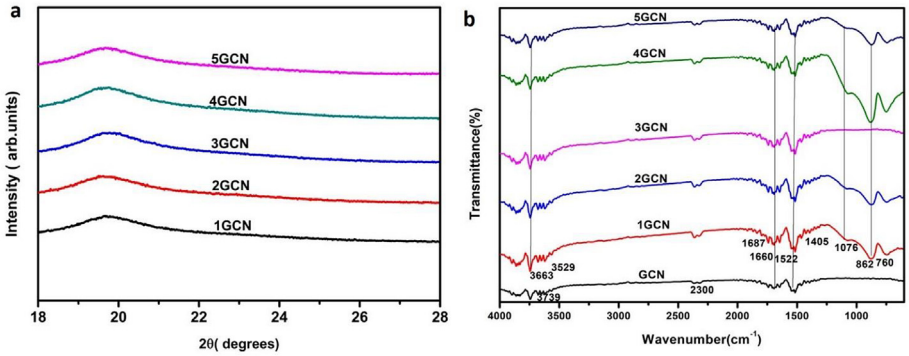

Figure 4. (a) XRD of the nanocomposite thin films, (b) FTIR of the nanocomposite thin films.

concentration of GCN, the absorbance is enhanced owing to the availability of more π-π* of GCN in the nanocomposite thin films. The transmittance of nanocomposite thin films is depicted in Figure 5b. The transmittance for 1GCN, 2GCN, 3GCN, 4GCN, and 5GCN are 84.3%, 77.8%, 74%, 69.9% and 63.8% respectively. More than 60% transparency in visible and near IR regions is observed and is adequate for transient electronics. Therefore, 5GCN can be employed as a possible candidate in flexible electronics.

The bandgap is another vital criterion for optoelectronic applications. Hence, the bandgap of the thin film was calculated using Eqs. (2) and (3) [31].

$$(\alpha h\nu)^2 = A(h\nu - Eg) \tag{2}$$

$$\alpha = \frac{1}{t}\left(\frac{ln1}{T}\right) \tag{3}$$

T = Transmittance, t = thickness of the thin film, hv –photon energy, α –absorbance co-efficient Eg – bandgap, A –constant. Figure 6a depicts the bandgap which was obtained by extrapolating the straight line $(\alpha h\nu)^2$ vs hv. The optical bandgap for 1GCN, 2GCN, 3GCN, 4GCN, and 5GCN are 3.24, 3.22, 3.07, 2.87 and 2.84 eV respectively. Pristine PVA thin film displayed a bandgap of 5.6 eV [40].

The addition of various concentrations of GCN to PVA reduced the bandgap gradually owing to the availability of more defect traps in between HOMO and LUMO of PVA. Therefore, a narrow bandgap of 2.84 eV was attained for 5GCN. 12.85% $NaNO_3$ was incorporated in PVA by Mohammed et al [41] and attained a bandgap of 5.05 eV. M.M. Abdelaziz et al. [42] added 25% $TiCl_3$ in PVA and observed a bandgap of 3.5 eV. On the other hand, O.G. Abdullah [43] added 0.04 M copper sulfide in PVA thin film and observed a bandgap of 4.77 eV. When compared with the literature, a low bandgap of 2.84 eV was attained for 5GCN in the present study.

3.2.4. Optical conductivity

The optical conductivity provides the electronic states in the thin film and it is calculated by using Eq. (4) [44].

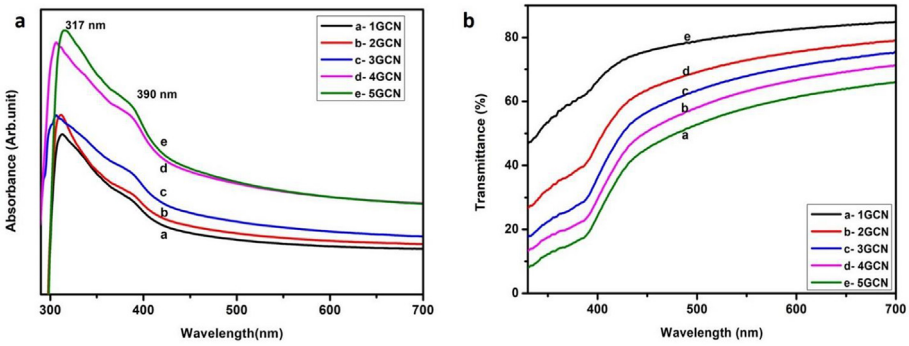

Figure 5. (a) Absorbance spectra of composite films. (b) Transmittance spectra of composite films.

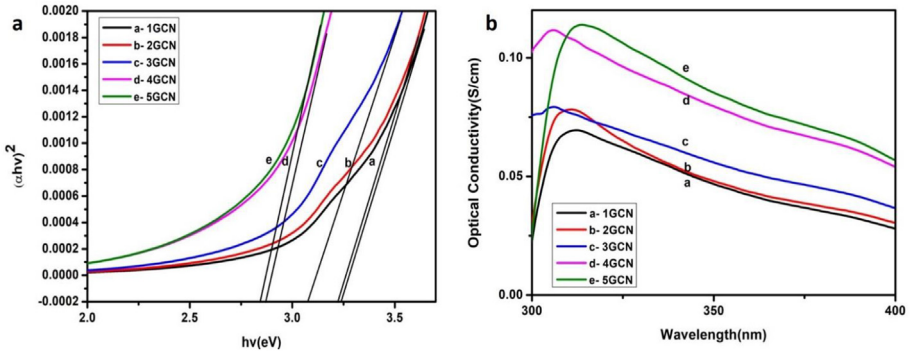

Figure 6. (a) Bandgap of the nanocomposite films, (b) Optical conductivity of the composite film.

$$\sigma = \frac{\alpha n c}{4\pi} \tag{4}$$

Figure 6b depicts the optical conductivity of the nanocomposite thin films. With the increase in the concentration of GCN, the optical conductivity increased gradually and attained a higher value for 5GCN. The increase in conductivity in 5GCN might be due to the availability of more charge carriers in the thin films. The optical properties of the nanocomposite thin films are shown in Table 2. As 5GCN depicts higher optical conductivity, there is a possibility that this composition can be utilized in optoelectronic applications.

3.2.5. Photoluminescence

Owing to the p-electron delocalization, polymers exhibit excellent luminescent properties. Due to these properties, it has found applications in light-emitting diodes and photodetectors. Hence it is significant to study the emission properties of the nanocomposite thin films. Figure 7a depicts the PL emission of the nanocomposite thin films which are excited at 325 nm. A blue emission peak at 440 nm is observed for all the thin films [32]. Srimathi et al [31] showed a sharp band at 280 nm for pure PVA thin film which might be due to the shift of electrons between LUMO to HOMO (π–π* transition). However, in the current study, no significant peak at 280 nm is observed. Owing to the formation of a new Vander Waal bond between –NH_2 of GCN and –OH of PVA, no significant peak is noticed at 280 nm. A new peak at 440 nm is noticed for the GCN-PVA nanocomposite thin films. With the increase in the concentration of GCN in PVA, the PL intensity increased with a blue shift noticed. When compared to 1GCN, 5GCN exhibited a two-fold enhancement in PL intensity. Due to the more defect centers in 5GCN, enhanced emission at 440 nm (2.8 eV) is noticed.

Table 2. Properties of the nanocomposite thin film.

Sample ID	Transmittance (%)	Bandgap (eV)	Optical conductivity(S)	Thickness (μm)
1GCN	84.3	3.24	0.069	20.5
2GCN	77.84	3.22	0.076	21
3GCN	74	3.07	0.079	20.3
4GCN	69.9	2.87	0.111	20.7
5GCN	63.8	2.84	0.113	20.9

3.2.5.1. Mechanism.

The mechanism for enhanced PL emission is shown in Figure 7b. The light is absorbed by the PVA polymer to create exciton (electron and holes). The electron that is generated is transferred from HOMO to LUMO of the polymer. Owing to the addition of GCN in PVA, more defect centers are created which traps the electron and delays the emission. The enhanced PL emission in 5GCN is due to the availability of more defect centers. The other description also specified that the formation of heterojunction between the GCN molecule and PVA matrix, decreased the recombination rate [Figure 8]. Light is absorbed by the PVA polymer and the excitons are generated. The generated electron is shifted from HOMO to LUMO. From LUMO the electron is shifted to LUMO of GCN. From LUMO the electron recombines with holes of GCN to generate emission. Owing to the charge transfer, the recombination rate is low and a high PL intensity is noticed for the thin films. Normally, the photoluminescence emission of PVA is due to the n-π* and π-π*. Generally, three processes such as non-radiative recombination, exciton recombination, and radiative trap recombination occur in PL emission [31]. Pristine GCN experiences radiative recombination [32]. In the present study, GCN exhibits higher PL emission, hence it undergoes emission by radiative recombination mechanism. Also, GCN shows enhanced PL emission at 450 nm, which is due to the π-π* bonds in GCN.

Hamzah et al [45] fabricated hydrothermal ZnO nanorod-based PVA-based nanofibers by electrospinning process and investigated the

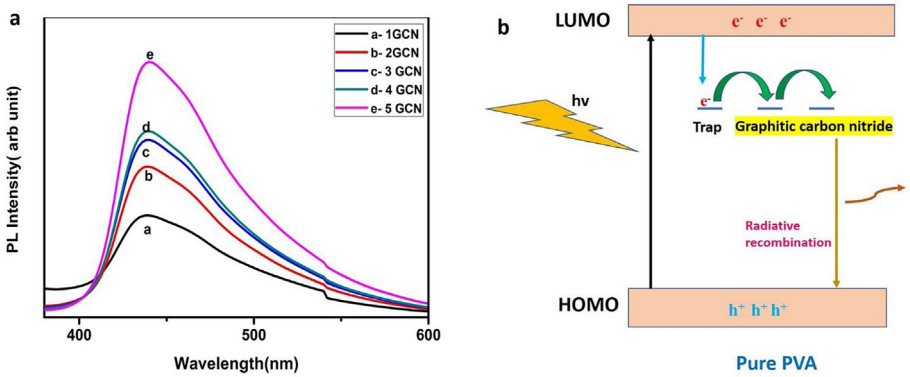

Figure 7. (a) Room-temperature PL emission of the nanocomposite thin film, (b) Schematic representation of the PL emission.

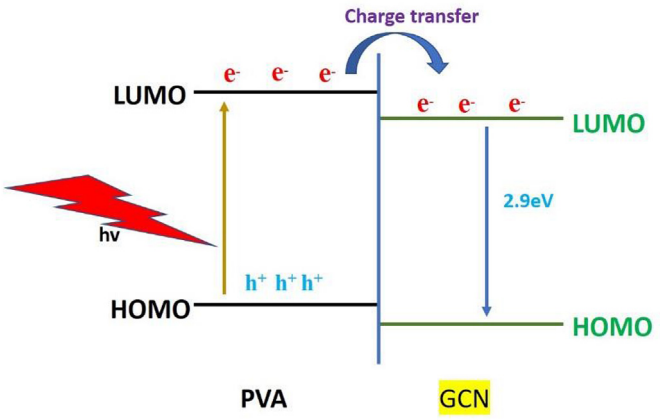

Figure 8. Schematic representation of charge separation of e^-/h^+ at the interface between PVA and GCN.

optical properties and found enhanced blue luminescence at 450 nm. Karthikeyan et al fabricated ZnO/PVA thin film by casting method and investigated the optical properties [38]. Three emissions were noticed by the composite thin film such as a UV emission peak at 380 nm, a blue emission peak at 450 nm, and green emission at 550 nm. In the present study, GCN/PVA emits purely 100% blue emission at 450 nm. Hence it can be employed in LEDs. As GCN is n-type material [34], with PVA it can serve as an electron transporter in organic solar cells. On the other hand, AlGaN thin film is used as a light source in LED which is costly and cumbersome to prepare [46]. Therefore, GCN/PVA could be a possible candidate to emit blue emissions in LEDs. Further, due to its transparent and flexible nature, this material is used to create various flexible electronics such as inverters, static random-access memories, gates, and ring oscillators.

3.2.6. Electrical conductivity

Four probe hall effect instrument is used to measure the electrical conductivity of the thin films. The electrical property is shown in Table 3. The conductivity increases as GCN increases in the PVA matrix. Due to the availability of more π-π * bonds in 5GCN, higher charge carriers are noticed in 5GCN. Regarding the mobility and average hall coefficient, a gradual increase in the values is noticed which may be attributed to the increasing concentration of GCN in the PVA matrix. However, the bulk and sheet concentration depicted an irregular trend which may be due to the agglomeration of GCN in PVA polymer. The higher conductivity is due to the low bandgap in the 5GCN nanocomposite thin film. 6% CuO was added to the PVA and found a conductivity of 3.62×10^{-8} S/cm [47]. Selvi et al [48] fabricated 6% ZnO/PVA nanocomposite thin film and found the electrical conductivity of 1.48×10^{-8} S/cm. Further 6% Fe_2O_3 was added in PVA and fabricated the thin film and found the electrical conductivity as 2.4×10^{-8} S/cm [49]. When compared with existing literature, GCN-doped PVA has higher conductivity due to the presence of more conjugated bonds. As 5GCN possesses higher PL emission, lower bandgap and higher conductivity, it was taken further to fabricate smart apparels.

3.3. Optical property of smart apparel

Different techniques have been implemented to embed nanomaterials in apparel [50]. Among them, solution blending is an easy and cost-effective method. Hence, we have adopted that technique to embed PVA/GCN in cotton cloth. The application of smart apparel is based on optical properties. Therefore, UV absorbance was studied for smart apparel. The UV absorbance of GCN/PVA has two peaks which are depicted in Figure 9a. One peak at 308 nm corresponds to the n-π* and π-π* transitions [38] and another peak at 400 nm is attributed to π-π* transitions of GCN. The photograph of GCN/PVA is shown in Figure 9b which depicts a neat embodiment of the nanocomposite on the cotton cloth. Generally, smart apparel is employed in the military to shield from extreme heat. Further, it can be used in optoelectronic devices for communicating between the soldiers. In the present study, a higher UV absorbance is noticed, hence it can be used to fabricate economical, flexible, biodegradable LED which might be beneficial for the military society. Further GCN is an n-type material hence it can serve as a photocatalyst in hydrogen production. Graphitic carbon nitride has high antibacterial activity [51], hence this smart apparel containing GCN can be used in wound dressing.

Table 3. Electrical properties of GCN/PVA thin film.

Sample Id.	Bulk conc. (cm^{-3})	(±SD)	Sheet conc. (cm^{-2})	(±SD)	Conductivity Scm^{-1}	(±SD)	Mobility (cm^2/Vs)	(±SD)	Average hall coefficient (Cm^3/C)	(±SD)
1GCN	2.6312×10^{14}	0.090×10^{14}	1.2037×10^{9}	0.149×10^{9}	4.3860×10^{-4}	0.283×10^{-4}	1.1582×10^{1}	0.137×10^{1}	2.5082×10^{4}	0.195×10^{4}
2GCN	1.5215×10^{14}	0.101×10^{14}	7.2364×10^{9}	0.151×10^{9}	4.6061×10^{-4}	0.161×10^{-4}	2.1818×10^{1}	0.144×10^{1}	4.4905×10^{4}	0.132×10^{4}
3GCN	3.5682×10^{11}	0.138×10^{11}	1.7306×10^{9}	0.098×10^{9}	5.395×10^{-4}	0.248×10^{-4}	9.5121×10^{3}	0.151×10^{3}	1.7566×10^{7}	0.075×10^{4}
4GCN	7.5075×10^{11}	0.095×10^{11}	3.6335×10^{8}	0.121×10^{8}	7.2634×10^{-4}	0.144×10^{-4}	6.03086×10^{3}	0.079×10^{3}	8.2617×10^{6}	0.116×10^{4}
5GCN	2.1502×10^{11}	0.151×10^{11}	1.1935×10^{9}	0.162×10^{9}	7.6462×10^{-3}	0.293×10^{-3}	2.5388×10^{4}	0.075×10^{4}	3.0432×10^{7}	0.115×10^{4}

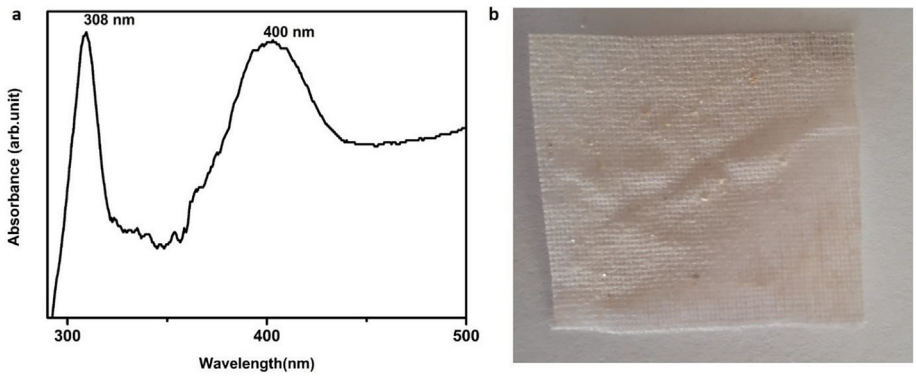

Figure 9. (a) UV absorbance of GCN/PVA on cotton fabric, (b) photograph of GCN/PVA on cotton cloth.

Generally, metal oxide such as TiO_2 owns self-cleaning properties in UV light [52] only. However, GCN covers 45% of solar light, hence it can self-clean in that region. In the previous study, PPy was incorporated into PVA and applied to apparel [53]. It is a P-type material, whereas, in the current study GCN is an n-type material. Therefore, smart apparel can be used as a candidate in the military community for textile and optoelectronic applications. Further, it can be used in the medical field as clothing for ICU patients who could not change their dressing.

4. Conclusion

A cost-effective smart fabric was prepared with graphitic carbon nitride and PVA polymer. The particle size analyzer confirmed the size of GCN in the nano dimension. The GCN embedment in the PVA matrix was affirmed by XRD and FTIR studies. The optical studies depicted a higher absorbance for 5GCN which might be due to the higher amount of GCN which in turn provides more unsaturated bonds in the thin film. Further, a low bandgap (2.84 eV) and higher transmittance (63.8%) were achieved for 5GCN thin film. The mechanism for higher PL intensity was explained. Higher optical and electrical conductivity was attained for 5GCN. As 5GCN has higher PL intensity and higher electrical conductivity, it was further taken to fabricate smart apparel. Further, according to literature, GCN possesses high antibacterial activity, hence it can serve as clothing for the military and medical community.

Declarations

Author contribution statement

Srimathi Krishnaswamy: Conceived and designed the experiments; Analyzed and interpreted the data; Wrote the paper.

Puspamitra Panigrahi, Praseetha Ramakrishnan, Ganapathi Subramanian Nagarajan: Contributed reagents, materials, analysis tools or data.

Sharon Sofini: Performed the experiments; Contributed reagents, materials, analysis tools or data.

Funding statement

This work was supported by Hindustan Institute of Technology and Science and by National Research Foundation of Korea (NRF) funded by the Ministry of Education, Science and Technology (MEST) (Grant No. 2013-044975 and Grant No. 2012-033431). The author NGS was supported by Dongguk University through QSRC and NITA.

Data availability statement

No data was used for the research described in the article.

Declaration of interests statement

The authors declare no conflict of interest.

Additional information

No additional information is available for this paper.

References

[1] X.M. Tao, Woodhead Publishing Limited, 2005.
[2] Z.T. Li, Z.L. Wang, Adv. Mater. 23 (2011) 84.
[3] K. Koski, A. Vena, L. Sydanheimo, L. Ukkonen, Y. Rahmat-Samii, IEEE Antenn. Wirel. Pr. 12 (2013) 964.
[4] F. Clemens, M. Wegmann, T. Graule, A. Mathewson, T. Healy, J. Donnelly, A. Ullsperger, W. Hartmann, C. Papadas, Adv. Eng. Mater. 5 (2003) 682.
[5] K. Laxminarayana, N. Jalili, Textil. Res. J. 75 (2005) 670.
[6] P. Xue, K.H. Park, X.M. Tao, W. Chen, X.Y. Cheng, Compos. Struct. 78 (2007) 271–277.
[7] Sun Hee Kim, Joo Hyeon Lee, J. Kor. Phys. Soc. 66 (2015) 629.
[8] H. Tao, et al., Proc. Natl. Acad. Sci. U.S.A. 111 (2014), 17385.
[9] S.M. Won, et al., Adv. Funct. Mater. 28 (2018), 1801819.
[10] J. Yoon, et al., ACS Nano 12 (2018) 6006.
[11] Lokanathan reddy, et al., J. Mater. Sci. Mater. Electron. 30 (2019) 1.
[12] N. Mahanta, S. Valiyaveettil, Nanoscale 3 (2011) 4625.
[13] R. Surkatti, M.H. El-Naas, J. Water Proc. Eng. 1 (2014) 84.
[14] L. Yin, et al., Adv. Funct. Mater. 24 (2014) 645.
[15] S.K. Kang, ACS Appl. Mater. Interfaces 7 (2015) 9297.
[16] L.C.-K. Liau, Y.-H. Lin, J. Lumin. 181 (2017) 217–222.
[17] E.N. Suchkova, et al., Russ. Phys. J. 51 (2008) 633–636.
[18] K.J. Ramalingam, et al., Synth. Met. 191 (2014) 113.
[19] X.M. Tao, Wearable Electronics and Photonics, Woodhead Publishing Limited, 2005.
[20] J. Zhang, et al., Angew. Chem. Int. Ed. 54 (2015) 6297–6301.
[21] Jinghai Liu, et al., J. Mater. Chem. 21 (2011), 14398.
[22] Y. Wang, et al., Angew. Chem., Int. Ed. 51 (2012) 68–89.
[23] M.J. Bojdys, J.O. Muller, et al., Chem. Eur J. 14 (2008) 8177–8182.
[24] Asif Hayat, et al., ACS Appl. Mater. Interfaces 11 (50) (2019) 46756–46766.
[25] Asif Hayat, et al., Catalysts 11 (2021) 935.
[26] Asif Hayat, et al., J. Colloid Interface Sci. 554 (2019) 627–639.
[27] Asif Hayat, et al., J. Colloid Interface Sci. 560 (2020) 743–754.
[28] Fan, et al., Chem. Phys. Lett. 699 (2018) 146.
[29] Danial Nemati, et al., Biotechnol. Progress (2021).
[30] Shaojian He, et al., Polymers 11 (2019) 610.
[31] K. Srimathi, et al., J. Mater. Sci. Mater. Electron. 31 (2020) 8502–8513.
[32] Yiming He, et al., Sol. Energy Mater. Sol. Cells 137 (2015) 175–184.
[33] Yuewei Zhang, et al., Nanoscale 4 (2012) 5300–5303.
[34] J. Fu, et al., Small 13 (2017), 1603938.
[35] S.C. Yan, et al., Langmuir 25 (2009) 10397–10401.
[36] J. Wang, W.D. Zhang, Electrochim. Acta 71 (2012) 10–16.
[37] J.X. Sun, et al., Dalton Trans. 41 (2012) 6756–6763.
[38] B. Karthikeyan, et al., Spectrochim. Acta-A: Mol. Biomol. Spec. 152 (2016) 485–490.
[39] D.M. Fernandes, et al., Mater. Chem. Phys. 128 (2011) 371–376.
[40] Muhammad Aslam, et al., Polymer Engineering and Science, 2018, pp. 2119–2132.
[41] F.F. Muhammad, S.B. Aziz, S.A. Hussein, J. Mater. Sci. Mater. Electron. 26 (2015) 521.
[42] M.M. Abdelaziz, M.M. Ghannam, Phys. B Condens. Matter 405 (2010) 958.
[43] O.G. Abdullah, S.A. Saleem, J. Electron. Mater. 45 (2016) 5910.
[44] J.V. Thombare, M.C. Rath, S.H. Han, et al., J. Semiconduct. 34 (2013) 93001–93006.
[45] M. Hamzah, et al., J. Mater. Sci. Mater. Electron. 28 (2017) 11915–11920.
[46] Y. Guo, et al., J. Nanophotonics 12 (2018), 043510.
[47] J. Selvi, et al., Polym. Compos. 40 (2019) 3737–3748.
[48] J. Selvi, et al., Iran. Polym. J. 29 (2020) 411–422.
[49] V. Parthasarathy, et al., Polym. Bull. 78 (2021) 2191.
[50] Ruckdashel, et al., J. Appl. Phys. 129 (2021), 130903.
[51] R. Nithya, et al., AIP Conf. Proc. 2270 (2020), 070002.
[52] Deyong Wu, ACS Appl. Mater. Interfaces 3 (12) (2011) 4770–4774.
[53] K. Srimathi, et al., Optik 266 (2022), 169596.